Supporting Information: A Hybrid-DFT Study of Intrinsic Point Defects in MX_2 (M=Mo, W; X=S, Se) Monolayers

A. Akkoush,[1,2] Yair Litman,[3] and M. Rossi[1,2]

[1] *Fritz Haber Institute of the Max Planck Society, Faradayweg 4–6, 14195 Berlin, Germany*
[2] *MPI for the Structure and Dynamics of Matter, Luruper Chaussee 149, 22761 Hamburg, Germany*
[3] *Yusuf Hamied Department of Chemistry, University of Cambridge, Lensfield Road, Cambridge, CB2 1EW,UK*

(Dated: April 28, 2023)

S1. SIMULATION DETAILS

A. Supercell Convergence

In order to identify the appropriate size of the supercell that prevents any potential interaction between defects, we have computed the formation energy difference of VX for the studied TMDC's with respect to various supercell sizes (fig.S1). The calculation is carried out using the PBE+MBD functional.

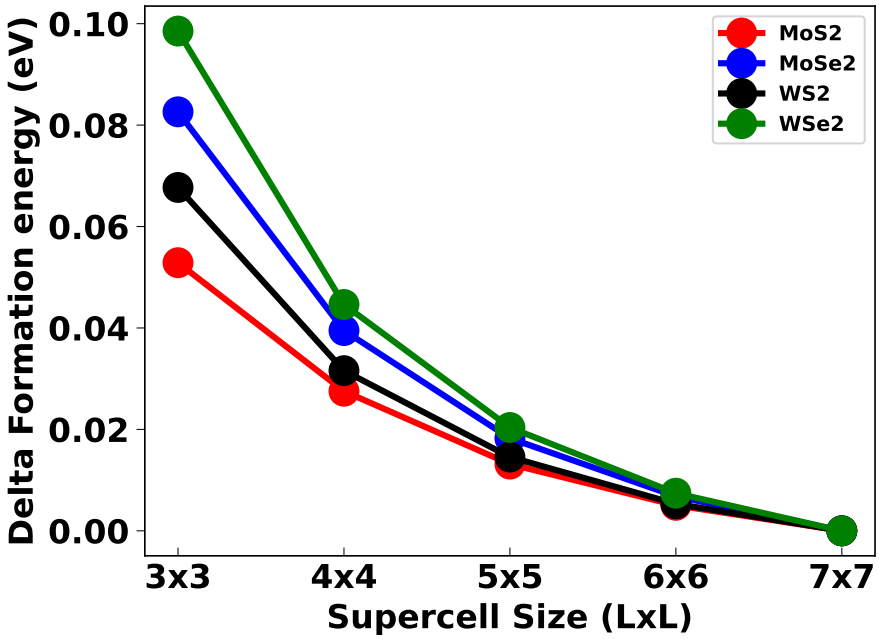

FIG. S1: Formation energy convergence of VX in MX_2 mono layers with supercell size.

B. Charge Correction

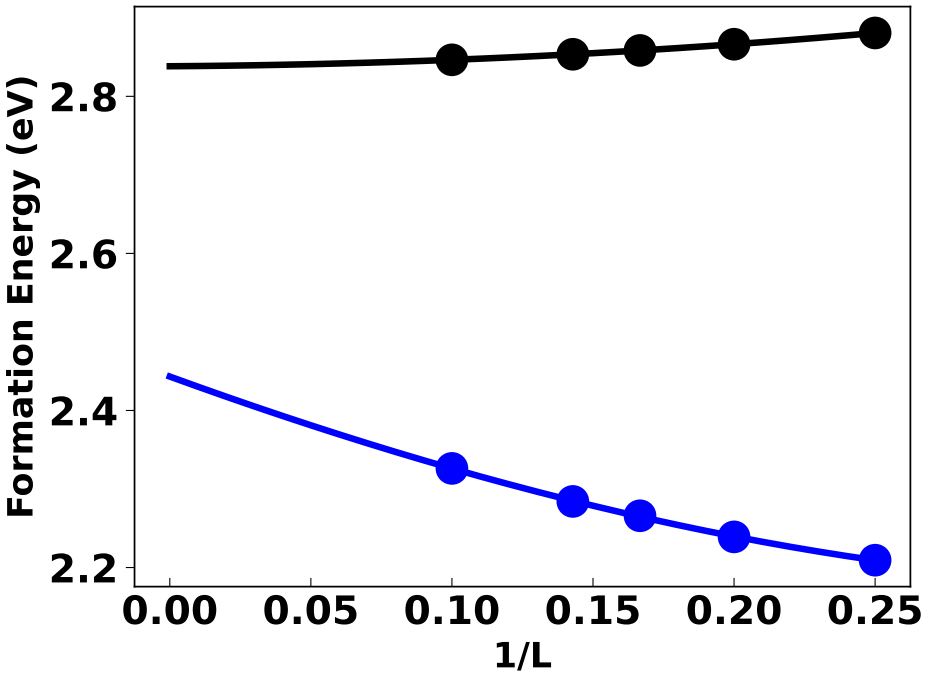

FIG. S2: Formation energy of VS (-1) in blue and neutral VS in black created in MoS_2 monolayer using PBE, calculated via the VCA. Solid lines show the defect formation energies extrapolated to the dilute limit of a single defect in an extended material ($1/L \to 0$) where L is the multiple of the lattice constant.

C. Structure Optimization

TABLE S1: Geometry Relaxation with HSE06+MBD, a. shows the bond length between X and its corresponding additional X atom on top, b. shows the change between $M - M$ bond lengths of the equilateral triangle upon the introduction of X vacancy.

(a)Add$X$

MoS_2	$MoSe_2$	WS_2	WSe_2
1.93	2.23	1.94	2.24

(b)VX

MoS_2	$MoSe_2$	WS_2	WSe_2
0.10	0.17	0.15	0.22

D. Cluster Search

Different cluster shapes and sizes have been investigated in our search to find an optimal structure. Mainly, we show three types of clusters with different edge atoms (fig.S3). We show in the table S3 the bandgap using HSE06 and PBE for these clusters. In this work we have considered the hexagonal structure with 43% S edges based on band gap calculations as in table S2. The cluster was passivated by hydrogens to ensure a higher band gap and no edge electron states dominance as shown for the chosen cluster S3.

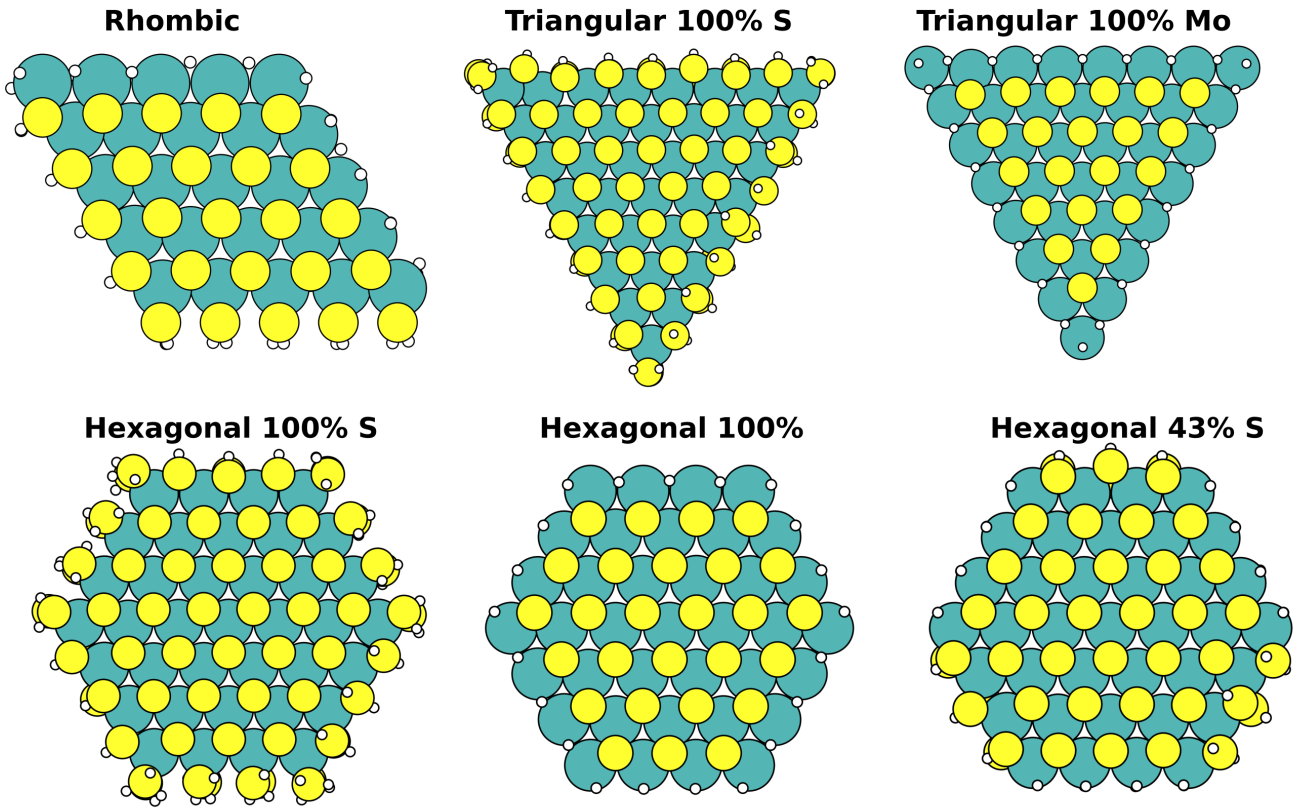

FIG. S3: MoS_2 cluster structures that has been investigated in this work

Systems	Rhombic 50% S	Triangular 100% S	Triangular 100% Mo	Hexagonal 100% S	Hexagonal 43% S (VS)	Hexagonal 100% Mo
E_{gap}[eV] (PBE)	0.139	0.045	0.024	0.014	0.226 (0.218)	0.0266
E_{gap}[eV] (HSE06)	0.093	0.141	0.177	0.030	0.676 (0.662)	0.274

TABLE S2: HOMO-LUMO bandgap of MoS_2 clusters using HSE06 and PBE functionals.

E. Band Gaps of Point Defects in MX_2

Systems	MoS_2	$MoSe_2$	WS_2	WSe_2
E_{gap}[eV] (PBE)	0.358	0.329	0.408	0.121
E_{gap}[eV] (HSE06)	0.694	0.621	0.871	0.730

TABLE S3: The bandgap variation between HSE06 and PBE of VM point defect in MX_2.

Systems	MoS_2	$MoSe_2$	WS_2	WSe_2
E_{gap}[eV] (PBE)	1.760	1.381	1.619	1.435
E_{gap}[eV] (HSE06)	2.194	1.935	2.242	1.813

TABLE S4: The bandgap variation between HSE06 and PBE of $AddX$ point defect in MX_2.

Systems	MoS_2	$MoSe_2$	WS_2	WSe_2
E_{gap}[eV] (PBE)	1.201	1.048	1.125	1.219
E_{gap}[eV] (HSE06)	1.768	1.546	1.736	1.475

TABLE S5: The bandgap variation between HSE06 and PBE of VX point defect in MX_2.

Systems	MoS_2	$MoSe_2$	WS_2	WSe_2
E_{gap}[eV] (PBE)	1.151	1.069	1.017	0.836
E_{gap}[eV] (HSE06)	1.688	1.512	1.603	1.374

TABLE S6: The bandgap variation between HSE06 and PBE of $VX2$ point defect in MX_2.

Systems	MoS_2	$MoSe_2$	WS_2	WSe_2
E_{gap}[eV] (PBE)	0.963	0.908	1.200	1.068
E_{gap}[eV] (HSE06)	1.525	1.458	1.675	1.440

TABLE S7: The bandgap variation between HSE06 and PBE of $VX22$ point defect in MX_2.

F. Impact of Temperature on the Formation Energy of Defects

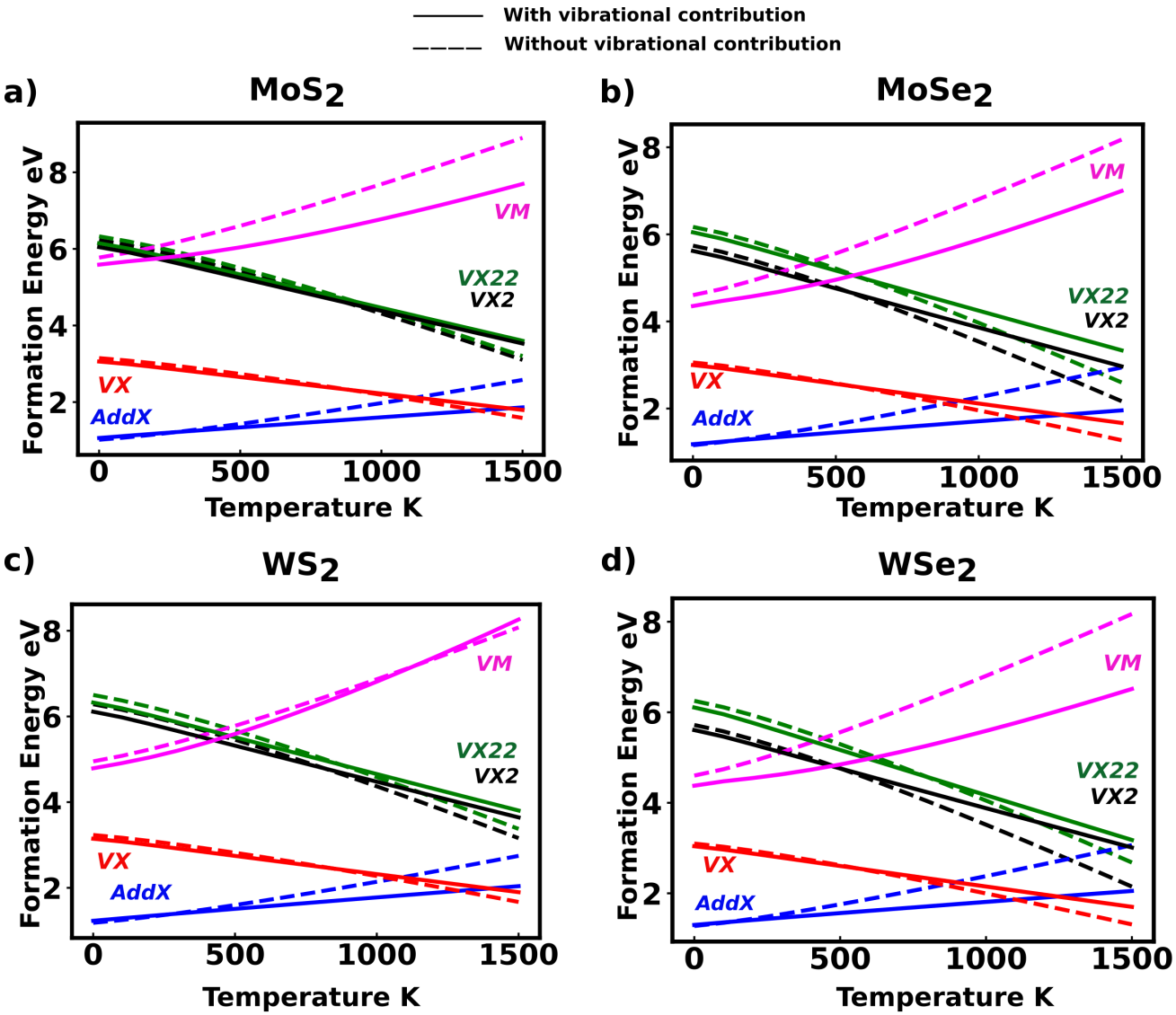

FIG. S4: Variation of formation energy (eV) of point defects for MX_2 monolayers as a function of temperature calculated with the HSE06+MBD functional at a S and Se partial pressure $p = 10^{-14}$ atm. The dashed lines represent the formation energy without the vibrational contribution $\Delta F(T)$ of the TMDCs and the solid lines the full formation energy.

G. Density of States of S Monovacancy in MoS_2 at Different Charge States

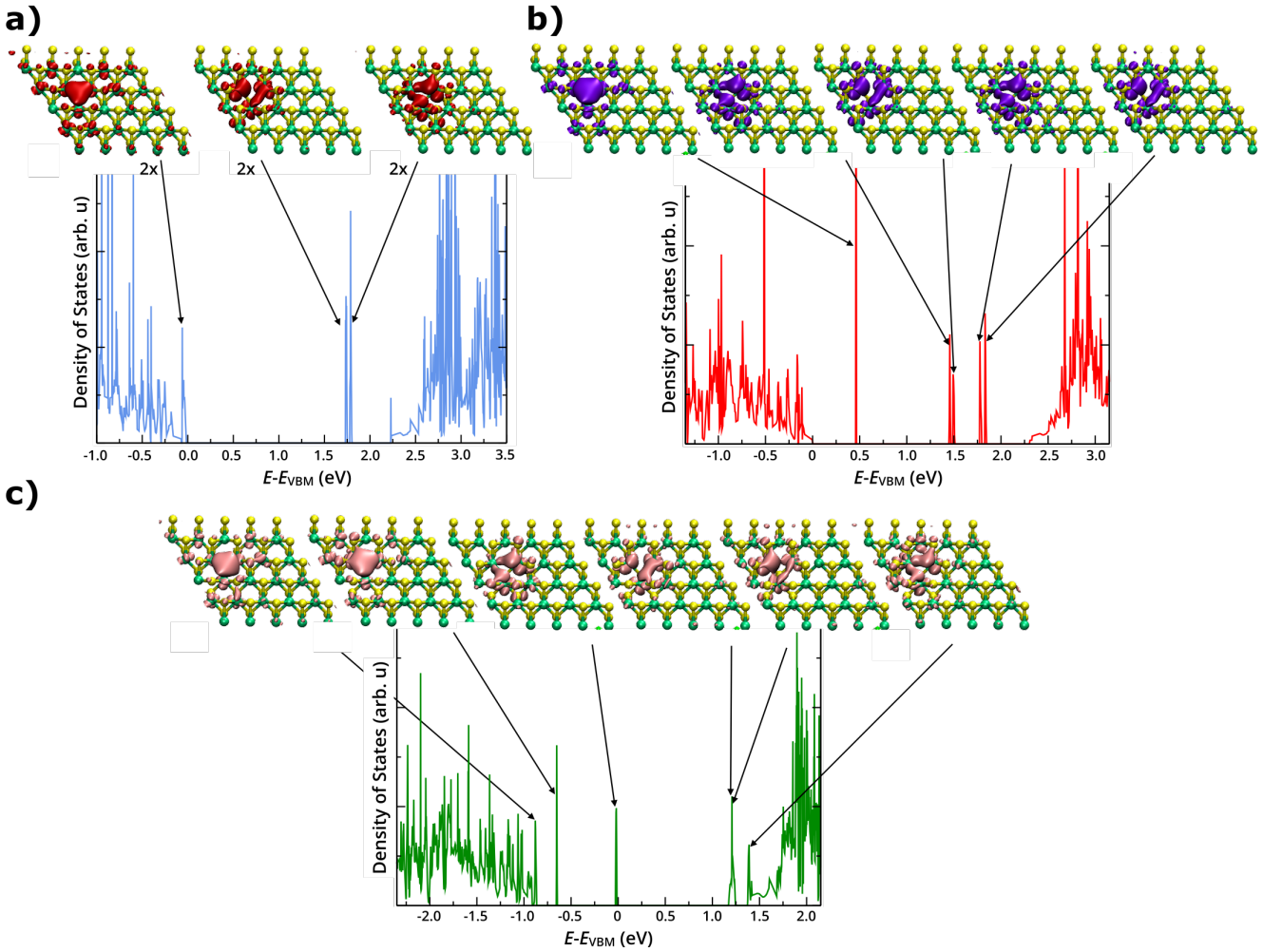

FIG. S5: Density of states and state-resolved electronic density of an MoS_2 monolayer containing (a) a neutral S monovacany, (b) a positively charged S monovacancy and (c) a negatively charged S monovacancy, employing the HSE06 functional and including SOC.

H. Density of States of Point Defects in MX_2 (HSE06)

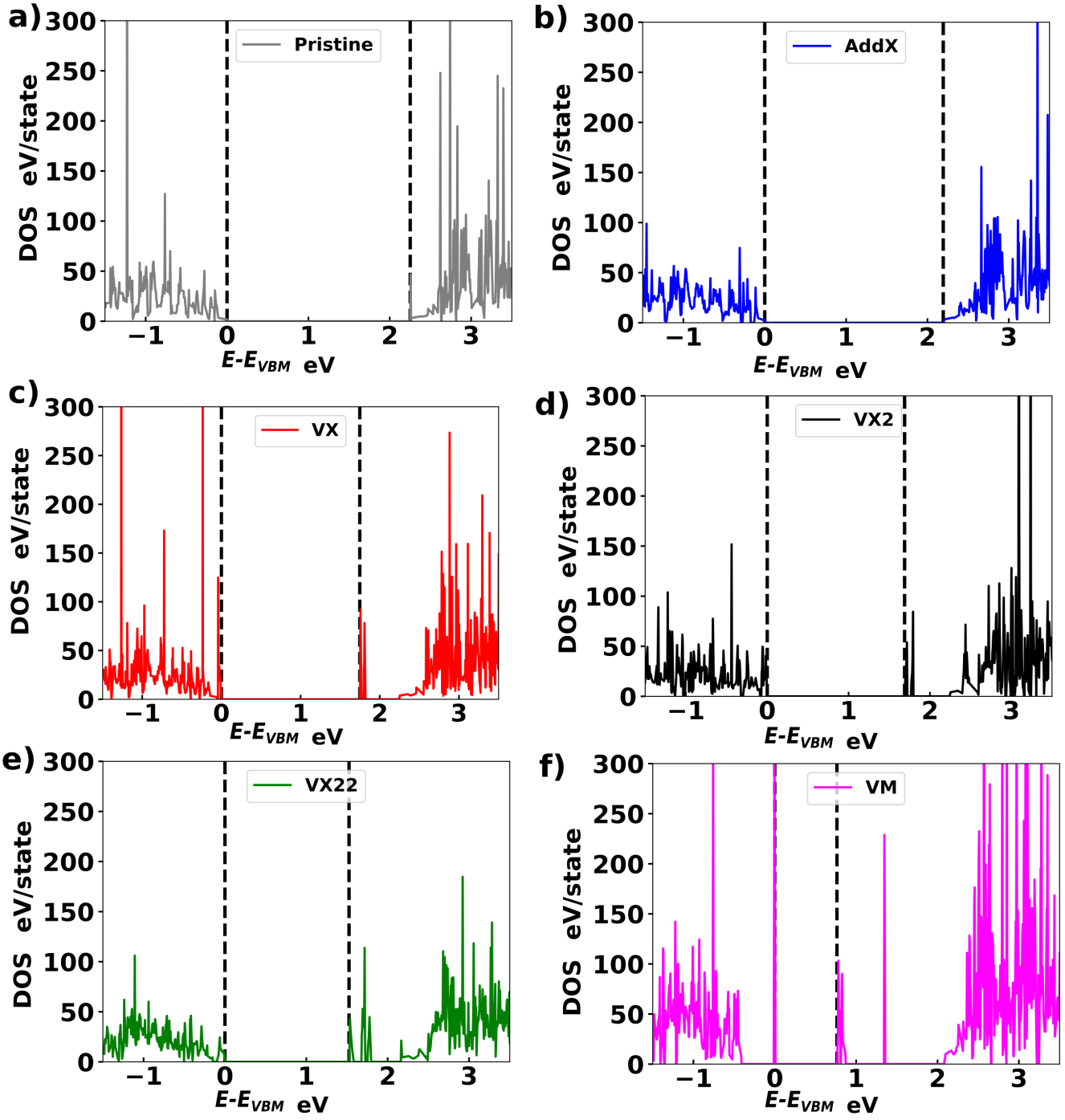

FIG. S6: Density of states of MoS_2 monolayer for the pristine and point defects under study using HSE06 exchange correlation and SOC.

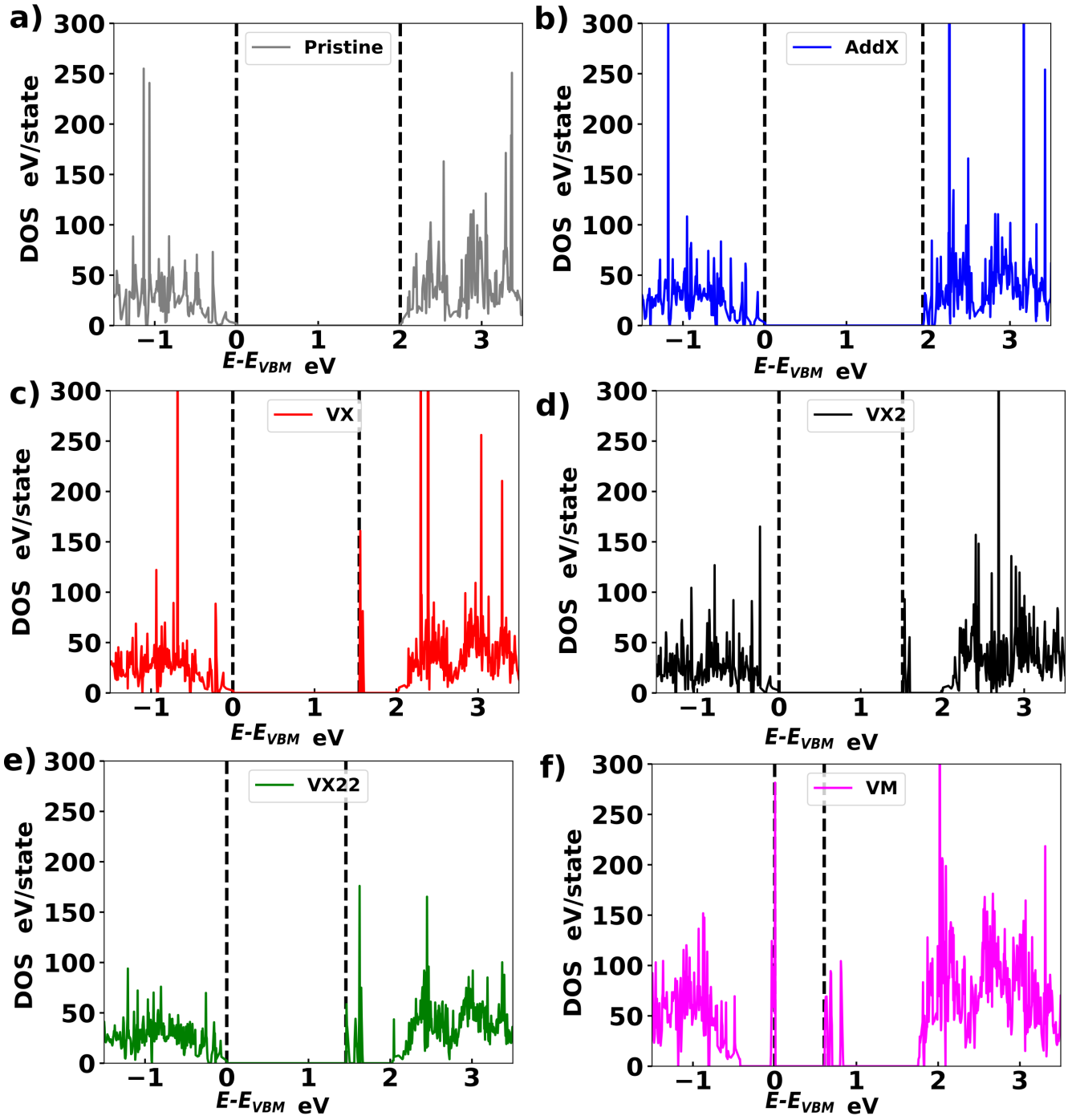

FIG. S7: Density of states of $MoSe_2$ monolayer for the pristine and point defects under study using HSE06 exchange correlation and SOC.

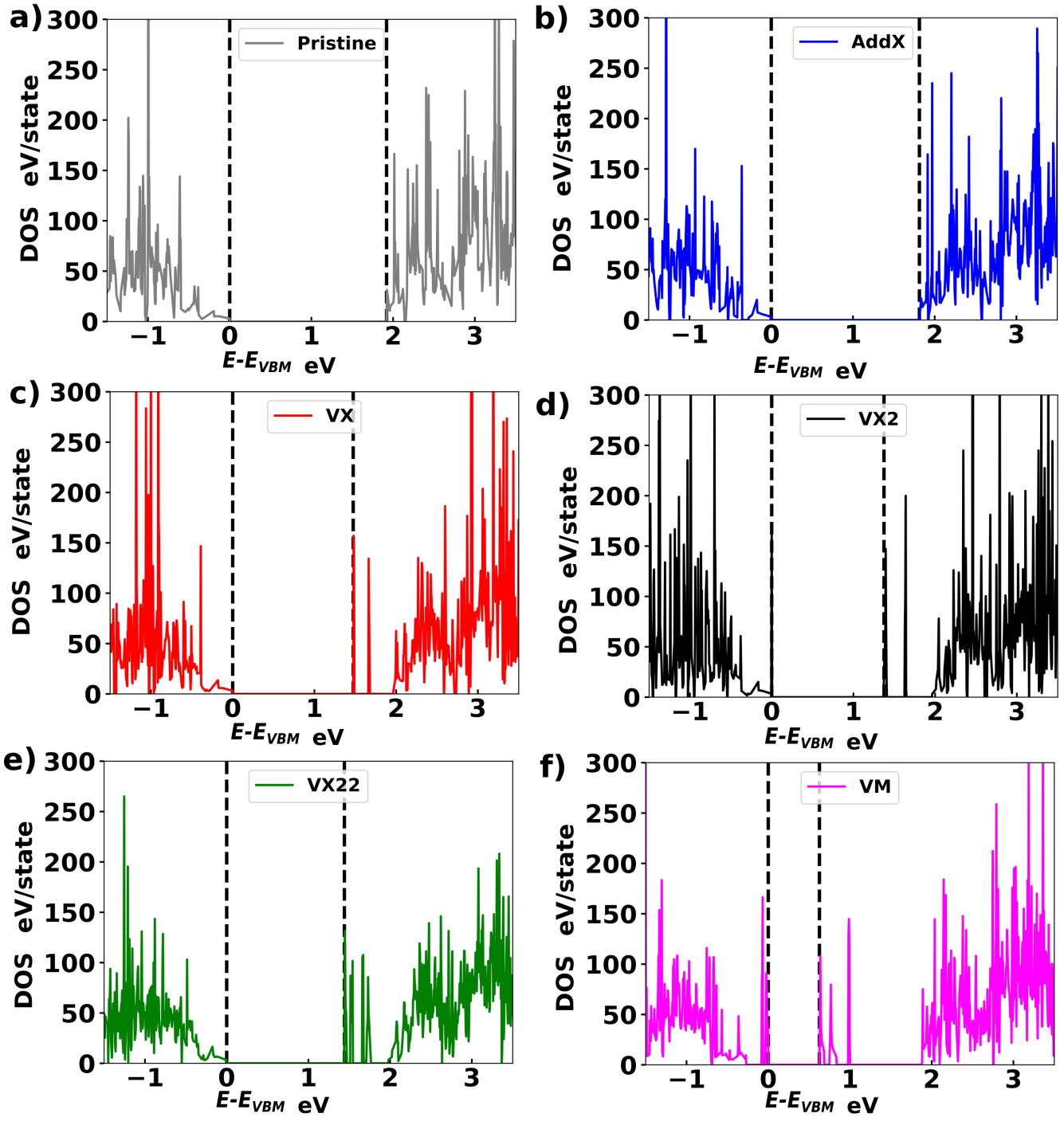

FIG. S8: Density of states of WS_2 monolayer for the pristine and point defects under study using HSE06 exchange correlation and SOC.

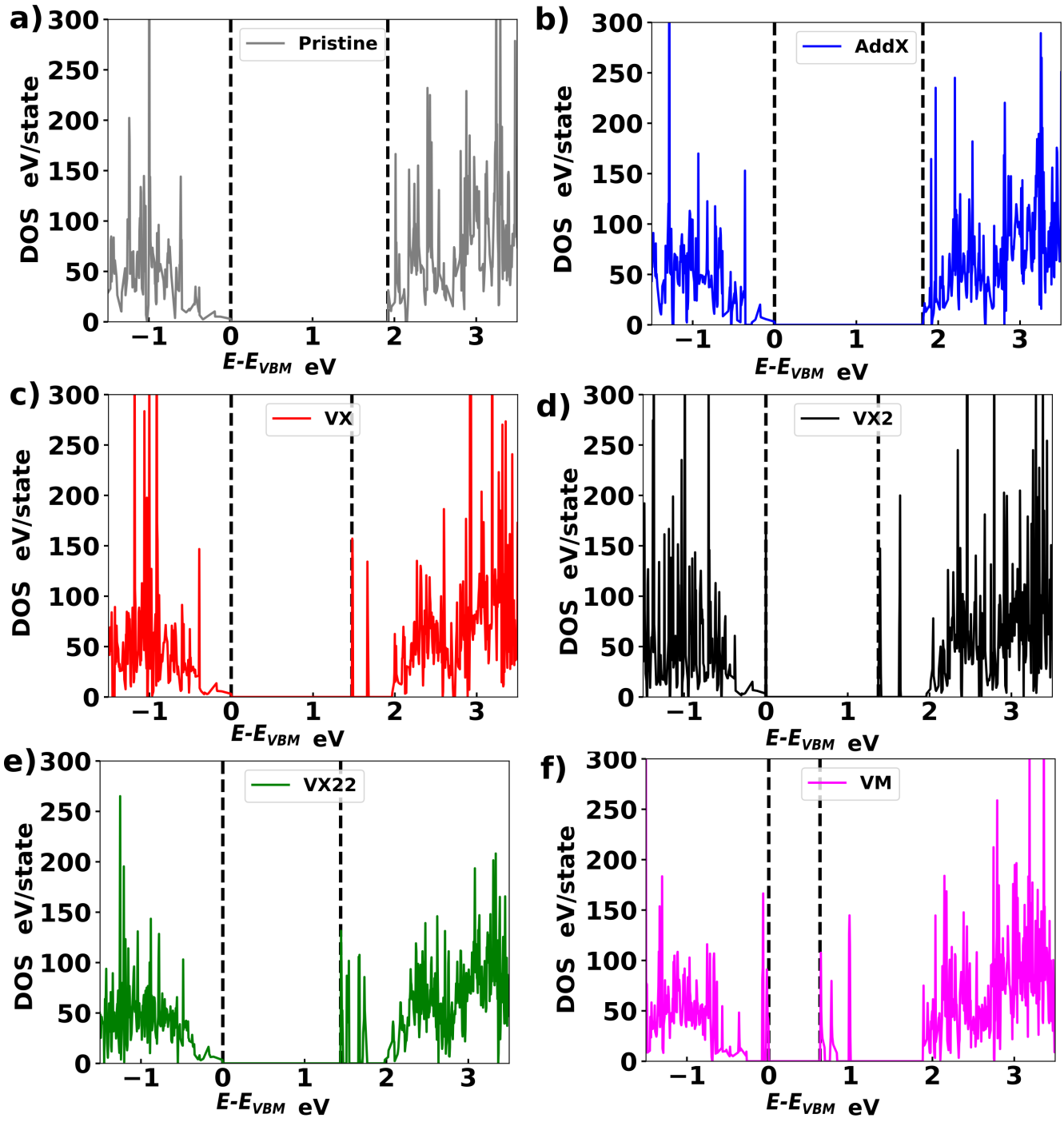

FIG. S9: Density of states of WSe_2 monolayer for the pristine and point defects under study using HSE06 exchange correlation and SOC.